Conformations of Unsolvated Valine-Based Peptides

Brian S. Kinnear, David T. Kaleta, Motoya Kohtani, Robert R. Hudgins,† and Martin F. Jarrold*

Contribution from the Department of Chemistry, Northwestern University, 2145 Sheridan Road, Evanston, Illinois 60208

Received April 6, 2000

Abstract: High-resolution ion mobility measurements and molecular dynamics (MD) simulations have been used to study the conformations of unsolvated valine-based peptides with up to 20 residues. In aqueous solution, valine is known to have a high propensity to form β-sheets and a low propensity to form α-helices. A variety of protonated valine-based peptides were examined in vacuo: Val_n+H^+, Ac-Val_n-Lys+H^+, Ac-Lys-Val_n+H^+, Val_n-Gly-Gly-Val_m+H^+, Val_n-^{L}Pro-Gly-Val_m+H^+, Val_n-^{D}Pro-Gly-Val_m+H^+, Ac-Val_n-Gly-Lys-Val_m+H^+, Ac-Val_n+H^+, and Arg-Val_n+H^+. Peptides designed to be β-hairpins were found to be random globules or helices. The β-hairpin is apparently not favored for valine-based peptides in vacuo, which is in agreement with the predictions of MD simulations. Peptides designed to be α-helices appear to be partial α/partial π-helices. Insertion of Gly-Gly, ^{L}Pro-Gly, or ^{D}Pro-Gly into the center of a polyvaline peptide disrupts helix formation. Some of the peptides that were expected to be random globules (because their most basic protonation site is near the N-terminus where protonation destabilizes the helix) were found to be helical with the proton located near the C-terminus. Helix formation appears to be more favorable in unsolvated valine-based peptides than in their alanine analogues. This is the reverse of what is observed in aqueous solution, but appears to parallel the helix propensities determined in polar solvents.

Introduction

Study of the factors responsible for the stability of α-helices[1] and β-sheets[2] has been an active research area for many years. Recently there has been growing interest in examining the conformations and properties of unsolvated peptides and proteins.[3−10] These vapor-phase studies can provide new insight into the role of intramolecular interactions and hydration interactions in determining the stability of the classic secondary structure elements. Our group studied helix formation in unsolvated alanine and glycine polypeptides. In solution, alanine has a high helix propensity,[11−13] and alanine-based peptides have been studied extensively.[14,15]

Despite alanine's high helix propensity in solution, protonated polyalanine peptides do not form helices in vacuo.[16,17] This is apparently because the N-terminus is protonated. Protonation at the N-terminus destabilizes the helix because the positive charge is at the positive end of the helix dipole.[18,19] On the other hand, unsolvated Ac-Ala_n-LysH^+ peptides, with a protonated lysine at the C-terminus, form stable helices for $n \geq 7$.[20,21] Here the helical conformation is stabilized by a favorable interaction between the charge (at the C-terminus) and the helix dipole[22,23] and by helix capping, in which the protonated amine on the lysine side chain hydrogen-bonds to the dangling backbone carbonyl groups at the C-terminus.[24−26]

In contrast to alanine, Ac-Gly_n-LysH^+ peptides are random globules in vacuo.[27] The failure to observe helices for Ac-Gly_n-

* To whom correspondence should be addressed.
† Present address: Institute for Physical Chemistry, University of Basel, Klingelbergstrasse 80, CH-4056 Basel, Switzerland.

(1) Chakrabartty, A.; Baldwin, R. L. *Adv. Protein Chem.* **1995**, *46*, 141−176.
(2) Smith, C. K.; Regan L. *Acc. Chem. Res.* **1997**, *30*, 153−161.
(3) Suckau, D.; Shi, Y.; Beu, S. C.; Senko, M. W.; Quinn, J. P.; Wampler, F. M.; McLafferty, F. W. *Proc. Natl. Acad. Sci. U.S.A.* **1993**, *90*, 790−793.
(4) Campbell, S.; Rodgers, M. T.; Marzluff, E. M.; Beauchamp, J. L. *J. Am. Chem. Soc.* **1995**, *117*, 12840−12854.
(5) Schnier, P. D.; Price, W. D.; Jockusch, R. A.; Williams, E. R. *J. Am. Chem. Soc.* **1996**, *118*, 7178−7189.
(6) Kaltashov, I. A.; Fenselau, C. *Proteins: Struct. Funct. Genet.* **1997**, *27*, 165−170.
(7) Valentine, S. J.; Clemmer, D. E. *J. Am. Chem. Soc.* **1997**, *119*, 3558−3566.
(8) Wyttenbach, T.; Bushnell, J. E.; Bowers, M. T. *J. Am. Chem. Soc.* **1998**, *120*, 5098−5103.
(9) Arteca, G. A.; Velázquez, I.; Reimann, C. T.; Tapia, O. *Phys. Rev. E* **1999**, *59*, 5981−5986.
(10) Schaaff, T. G.; Stephenson, J. L.; McLuckey, S. L. *J. Am. Chem. Soc.* **1999**, *121*, 8907−8919.
(11) Lyu, P. C.; Liff, M. I.; Marky, L. A.; Kallenbach, N. R. *Science* **1990**, *250*, 669−673.
(12) O'Neil, K. T.; DeGrado, W. F. *Science* **1990**, *250*, 646−651.
(13) Padmanabhan, S.; Marqusee, S.; Ridgeway, T.; Laue, T. M.; Baldwin, R. L. *Nature* **1990**, *344*, 268−270.
(14) Rohl, C. A.; Fiori, W.; Baldwin, R. L. *Proc. Natl. Acad. Sci. U.S.A.* **1999**, *96*, 3682−3687.
(15) Spek, E. J.; Olson, C. A.; Shi, Z. S.; Kallenbach, N. R. *J. Am. Chem. Soc.* **1999**, *121*, 5571−5572.
(16) Hudgins, R. R.; Mao, Y.; Ratner, M. A.; Jarrold, M. F. *Biophys. J.* **1999**, *76*, 1591−1597.
(17) Samuelson, S.; Martyna, G. J. *J. Phys. Chem. B* **1999**, *103*, 1752−1766.
(18) Ihara, S.; Ooi, T.; Takahashi, S. *Biopolymers* **1982**, *21*, 131−145.
(19) Shoemaker, K. R.; Kim, P. S.; York, E. J.; Stewart, J. M.; Baldwin, R. L. *Nature* **1987**, *326*, 563−567.
(20) Hudgins, R. R.; Ratner, M. A.; Jarrold, M. F. *J. Am. Chem. Soc.* **1998**, *120*, 12974−12975.
(21) Hudgins, R. R.; Jarrold, M. F. *J. Am. Chem. Soc.* **1999**, *121*, 3494−3501.
(22) Blagdon, D. E.; Goodman, M. *Biopolymers* **1975**, *14*, 241−245.
(23) Daggett, V. D.; Kollman, P. A.; Kuntz, I. D. *Chem. Scr.* **1989**, *29A*, 205−215.
(24) Presta, L. G.; Rose, G. D. *Science* **1988**, *240*, 1632−1641.
(25) Forood, B.; Feliciano, E. J.; Nambiar, K. P. *Proc. Natl. Acad. Sci. U.S.A.* **1993**, *90*, 838−842.
(26) Seale, J. W.; Srinivasan, R.; Rose, G. D. *Protein Sci.* **1994**, *3*, 1741−1745.

10.1021/ja001207v CCC: $19.00
Published on Web 09/09/2000

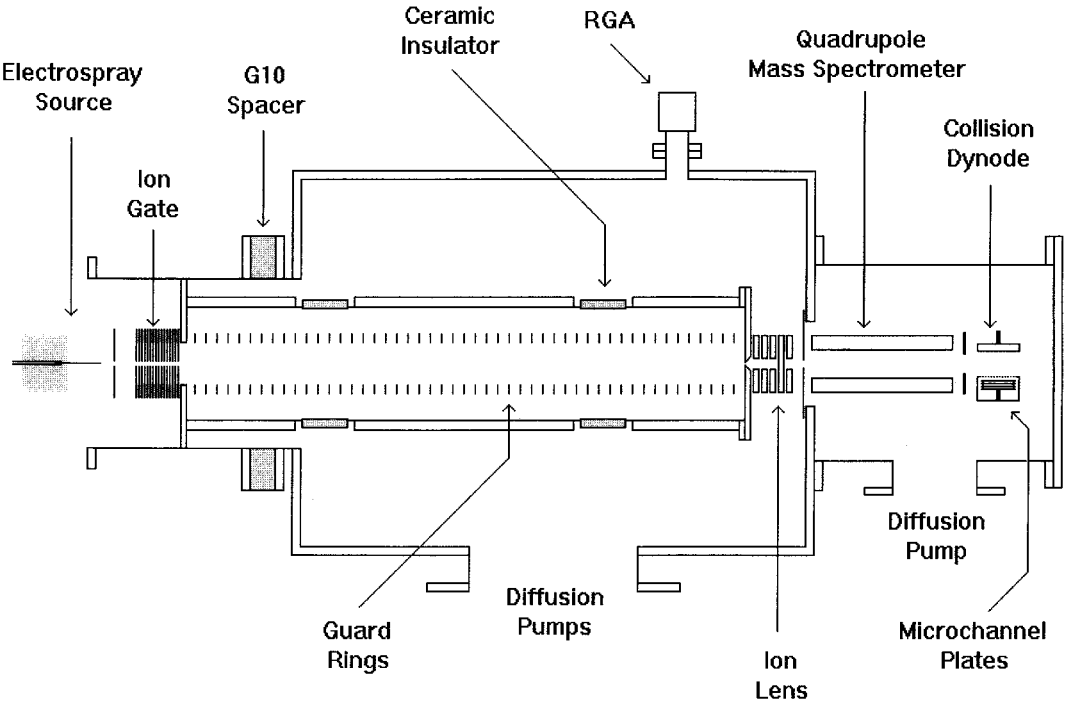

Figure 1. Schematic diagram of the experimental apparatus.

$LysH^+$ peptides, while Ac-Ala_n-$LysH^+$ peptides are helical, is consistent with solution-phase helix propensities.[1] The helix disruptive potential of glycine in aqueous solution appears to be partly due to the absence of a side chain, allowing solvent access to the polar groups along the helix backbone.[28] However, the primary cause of the low helix propensity of glycine in solution has been attributed to backbone entropy.[29,30] With no side chain, glycine can sample more conformational space than the other amino acids, so the entropy cost of helix formation is larger. According to calculations, the enthalpy difference between the helix and random globule is smaller for Ac-Gly_n-$LysH^+$ than it is for Ac-Ala_n-$LysH^+$ because glycine makes more compact and more stable random globules, and this also helps to make the helix unfavorable for glycine-based peptides in vacuo.[27]

In this manuscript, we report studies of the conformations of valine-based peptides. In aqueous solution, the helix propensity of valine is almost as low as glycine.[1] However, for valine, which has a bulky isopropyl side chain, the low solution-phase helix propensity has been attributed to side chain entropy or crowding: the helical geometry restricts the conformations available to the side chain, and this leads to an increased entropy cost for helix formation.[31] Thus, valine-based peptides might be thought to be unlikely to form helices in vacuo.

Although valine has a low propensity to form α-helices, it has a high propensity to form β-sheets. There have been several measurements of the β-sheet propensities of the naturally occurring amino acids, and valine is near the top in all of them.[2,32−34] The small valine-based peptides considered here may form β-hairpins. A β-hairpin, consisting of a turn and two short antiparallel β-strands, can be viewed as a model fragment of a β-sheet. β-hairpins are much less well-understood than α-helices. β-hairpins that are stable as monomers in aqueous solution were only identified relatively recently.[35,36] There is currently considerable interest in the kinetics and dynamics of β-hairpin formation.[37−39]

In the work described here, unsolvated peptide ions are generated by electrospray, and information about their conformations is obtained from high-resolution ion mobility measurements.[40] Mass spectrometry is used to select specific peptides for the mobility measurements. Ion mobilities depend on the collision cross-section, which in turn depends on the geometry.[41−43] Structural information is obtained by comparing the cross-sections derived from the mobilities to cross-sections calculated for trial geometries obtained from MD simulations. We have already shown that this approach can distinguish helices and random globules.[16]

Materials and Methods

Ion Mobility Measurements. Figure 1 shows a schematic diagram of the experimental apparatus. The apparatus is similar to that described in detail elsewhere,[40,44] except that the interface between the electrospray

(27) Hudgins, R. R.; Jarrold, M. F. *J. Phys. Chem. B* **2000**, *104*, 2154−2158.
(28) Luo, P.; Baldwin, R. L. *Proc. Natl. Acad. Sci. U.S.A.* **1999**, *96*, 4930−4935.
(29) Gō, M.; Gō, N.; Scheraga, H. *J. Chem. Phys.* **1970**, *52*, 2060−2079.
(30) Okamoto, Y.; Hansmann, U. H. E. *J. Phys. Chem.* **1995**, *99*, 11276−11287.
(31) Creamer, T. P.; Rose, G. D. *Proc. Natl. Acad. Sci. U.S.A.* **1992**, *89*, 5937−5941.
(32) Kim, C. A.; Berg, J. M. *Nature* **1993**, *362*, 267−270.
(33) Minor, D. L.; Kim, P. S. *Nature* **1994**, *371*, 264−267.
(34) Smith, C. K.; Withka, J. M.; Regan, L. *Biochemistry* **1994**, *33*, 5510−5517.
(35) Blanco, F. J.; Jiménez, M. A.; Herranz, J.; Rico, M.; Santoro, J.; Nieto, J. L. *J. Am. Chem. Soc.* **1993**, *115*, 5887−5888.
(36) Blanco, F. J.; Rivas, G.; Serrano, L. *Nat. Struct. Biol.* **1994**, *1*, 584−590.
(37) Muñoz, V.; Thompson, P. A.; Hofrichter, J.; Eaton, W. A. *Nature* **1997**, *390*, 196−199.
(38) Dinner, A. R.; Lazaridis, T.; Karplus, M. *Proc. Natl. Acad. Sci. U.S.A.* **1999**, *96*, 9068−9073.
(39) Kolinski, A.; Ilkoski, B.; Skolnick, J. *Biophys. J.* **1999**, *77*, 2942−2952.
(40) Dugourd, Ph.; Hudgins, R. R.; Clemmer, D. E.; Jarrold, M. F. *Rev. Sci. Instrum.* **1997**, *68*, 1122−1129.
(41) Hagen, D. F. *Anal. Chem.* **1979**, *51*, 870−874.
(42) von Helden, G.; Hsu, M.-T.; Kemper, P. R.; Bowers, M. T. *J. Chem. Phys.* **1991**, *95*, 3835−3837.
(43) Clemmer, D. E.; Jarrold, M. F. *J. Mass Spectrom.* **1997**, *32*, 577−592.

source and the drift tube has been modified to increase the signal intensity. The electrospray emitter is a 2-cm length of 400 μm OD 250 μm ID deactivated fused-silica capillary tubing. The emitter is held at 5 kV with respect to the stainless steel plate which is 0.5 cm away. The front plate contains a 0.5-cm aperture, and there is a voltage drop of 1410 V across the 2.5-cm gap between the front plate and the ion gate. The ion gate is a 5-cm-long stack of plates (with 0.5-cm apertures) separated by Teflon spacers and viton O-rings. The plates are connected to a voltage divider to generate a uniform field of 556 Vcm^{-1}. The drift tube contains helium buffer gas at slightly above atmospheric pressure so that there is a 2000 sccm flow of helium out of the drift tube and through the apertures in the ion gate. The electric field in the ion gate transports ions against the buffer gas flow and into the drift tube. However, the buffer gas flow prevents neutral molecules from entering the drift tube. This is confirmed by monitoring the gas which exits at the other end of the drift tube by using a residual gas analyzer. With adequate helium buffer gas flow through the ion gate, the amounts of O_2, N_2, and H_2O in the buffer gas in the drift tube can be maintained at close to or below 1 ppm (which is comparable to the impurity levels in the helium measured when the entrance to the drift tube is completely closed-off).

The second-to-last plate in the ion gate is divided into two parts and acts as an electrostatic shutter. With ~300 V across these plates, ions are not transmitted. The shutter is used to control the ions for drift time measurements. Drift times can be determined by stopping all the ions and then admitting a short (~1 ms) pulse and determining their arrival time at the detector. Drift times can also be obtained in a depletion mode in which ions are admitted continuously, except for a short time (~1ms) when the signal is pulsed off by the shutter. The drift tube is 63 cm long and has a uniform electric field along its length. The field is provided by 46 guard rings connected to a voltage divider. A drift voltage of 10 000 V was used. Ions travel along the length of the drift tube,and then a small fraction exit through a 0.125-mm aperture and enter the main vacuum chamber. The pressure in the main chamber is $\sim 10^{-4}$ Torr. Ions that exit the drift tube are focused through an aperture into a differentially pumped chamber (operating pressure $<10^{-6}$ Torr) where they enter a quadrupole mass spectrometer. After mass analysis, the ions are detected by an off-axis collision dynode and dual microchannel plates. Arrival-time distributions are recorded by a multichannel scaler which is synchronized with the electrostatic shutter that controls the ions entering the drift tube. Drift-time distributions are obtained by correcting the arrival times for the time that the ions spend traveling from the drift tube to the detector. The drift times are converted to collision cross-sections using[45] (Mason and McDaniel, 1988)

$$\Omega_{\text{avg}}^{(1,1)} = \frac{(18\pi)^{1/2}}{16}\left[\frac{1}{m} + \frac{1}{m_b}\right]^{1/2} \frac{z_e}{(k_B T)^{1/2}} \frac{t_D E}{L} \frac{1}{\rho} \qquad (1)$$

In this expression, m and m_b are the masses of the ion and buffer gas, z_e is the charge on the ion, ρ is the buffer gas number density, L is the length of the drift tube, and E is the drift field.

Peptide Synthesis. Except for one sample of Ac-Val_{19}-Lys which was synthesized by Anaspec (Anaspec Inc., San Jose, CA) and used without further purification, all the other peptides used in this work were synthesized using Fmoc chemistry on a Millipore 9050 Plus PepSynthesizer. After cleaving from the column with a 95% TFA (trifluoroacetic acid)/5% water cocktail, the peptides were washed in water and lyophilized. The solutions for electrospraying were prepared by dissolving 1 mg of peptide in 1 mL of TFA and 0.1 mL of water. The mass spectra show that there is a distribution of peptide sizes present, partly because of imperfect coupling in the synthesis and partly because the peptides slowly hydrolyze in the TFA that is used to dissolve them.

Molecular Dynamics Simulations. Molecular dynamics simulations were performed to derive cross-sections for comparison to the experimental results. The simulations were performed using the MACSIMUS suite of programs[46] employing CHARMM-like potentials (21.3 parameter set).[47] This force field is parametrized for proteins and peptides and includes electrostatic, van der Waals, and internal energy terms. Hydrogen bonds are incorporated in the electrostatic term. The internal energy term results from a distortion of the chemical bonds (length, angle, dihedral angle, and improper torsion) from their most favorable conformations. The bond lengths were constrained by SHAKE,[48] and the CH, CH_2, and CH_3 groups were treated as united atoms.[49] A time step of 1 fs was used, along with a dielectric constant of 1 (which is appropriate for small isolated peptides). A variety of starting conformations were employed: α-helix, β-hairpin, and a fully extended all-trans geometry. Most of the simulations either were run for 960 ps at 300 K or employed simulated annealing. A variety of simulated annealing schedules were tried. A schedule of 240 ps at 600, 500, and 400 K, followed by 480 ps at 300 K, was employed for most of the work described here. The temperature was maintained by rescaling the kinetic energies every 0.1 ps. Average energies and the structures for the cross-section calculations were derived from the last 35 ps of each simulation.

Cross-Section Calculations. Structural information is deduced by comparing the measured cross-sections to cross-sections derived from the MD simulations. The cross-section (or, more correctly, the collision integral) should be calculated by averaging the momentum transfer cross-section over relative velocity and collision geometry.[50] However, this requires trajectory calculations to evaluate the scattering angle (the angle between the incoming and outgoing trajectories in a collision between the ion and a buffer gas atom), which consumes large amounts of computer time.

Another approach to calculating cross-sections, the exact-hard-spheres scattering model,[51] ignores the intermolecular interactions but treats the scattering process between the ion and buffer gas atom correctly within the hard-sphere limit. This approach requires much less computer time than the trajectory method. Cross-sections calculated by the exact-hard-spheres scattering model are generally larger than those obtained by the trajectory method. The relative deviation is worse for small ions.

We have calculated cross-sections by the trajectory method and the exact-hard-sphere scattering model for a variety of peptides and proteins. By comparing the two data sets, an empirical correction to the cross-sections calculated by the exact-hard-spheres scattering model was derived. The empirical correction is given by

$$\Omega_{\text{CCS}} = a + b\cdot\Omega_{\text{EHSS}} + c\cdot\Omega_{\text{EHSS}}^2 + d\cdot(\Gamma - 1) + e\cdot z \qquad (2)$$

where Ω_{CCS} is the corrected cross-section, Ω_{EHSS} is the cross-section calculated by the exact-hard-spheres scattering model, Γ is an asymmetry parameter that measures how distorted the geometry is from spherical, and z is the charge. Γ is given by

$$\Gamma = \text{maximum value of}\left[\frac{\pi}{4}\frac{\sum xyz}{\sum yz}\right] \qquad (3)$$

where x, y, and z are the atomic coordinates. The coefficients a, b, c, d, and e were obtained from a least-squares fit. The root-mean-square deviation between the empirically corrected cross-sections and cross-sections calculated by the trajectory method is 0.42%. Most of the calculated cross-sections reported here were obtained using the empirically corrected exact-hard-spheres scattering model. Because the

(44) Hudgins, R. R.; Woenckhaus, J.; Jarrold, M. F. *Int. J. Mass. Spectrom. Ion. Proc.* **1997**, *165/166*, 497−507.

(45) Mason, E. A.; McDaniel, E. W. *Transport Properties of Ions in Gases*; Wiley: New York, 1988.

(46) Kolafa, J. http://www.icpf.cas.cz/jiri/macsimus/default.htm

(47) Brooks, B. R.; Bruccoleri, R. E.; Olafson, B. D.; States, D. J.; Swaminathan, S.; Karplus, M. *J. Comput. Chem.* **1983**, *4*, 187−217.

(48) Van Gunsteren, W. F.; Berendsen, H. J. *Mol. Phys.* **1977**, *34*, 1311−1327.

(49) Weiner, S. J.; Kollman, P. A.; Case, D. A.; Singh, U. C.; Ghio, C.; Alagona, G.; Profeta, S.; Weiner, P. *J. Am. Chem. Soc.* **1984**, *106*, 765−784.

(50) Mesleh, M. F.; Hunter, J. M.; Shvartsburg, A. A.; Schatz, G. C.; Jarrold, M. F. *J. Phys. Chem.* **1996**, *100*, 16082−16086.

(51) Shvartsburg, A. A.; Jarrold, M. F. *Chem. Phys. Lett.* **1996**, *261*, 86−91.

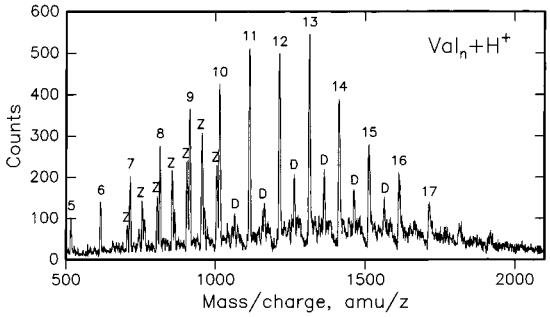

Figure 2. Electrospray mass spectrum measured for unpurified Val_{20} (1 mg in 1 mL of TFA and 0.1 mL of water). The peaks labeled with numbers correspond to Val_n+H^+ with $n = 5-17$. The peaks labeled Z correspond to Val_n+2H^+ and the peaks labeled D correspond to $Val_n+Val_m+2H^+$ with $n + m =$ odd.

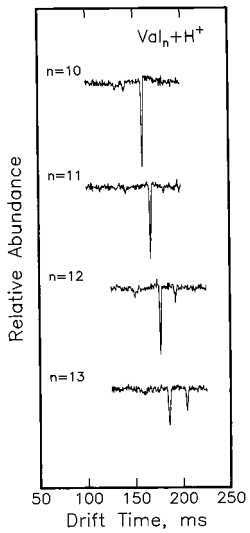

Figure 3. Drift-time distributions measured for Val_n+H^+ peptides with $n = 10-13$.

structure fluctuates during the MD simulations, average cross-sections were obtained by calculating cross-sections for 50 snapshots equally spaced over the last 35 ps of each MD simulation. If the conformations derived from the MD simulations are correct, the measured and calculated cross-sections are expected to agree within 1−2%.[52]

Results

Val_n+H^+ Peptides. Figure 2 shows an electrospray mass spectrum for unpurified Val_{20}. The series of peaks labeled with numbers correspond to singly protonated monomers, Val_n+H^+ with $n = 5-17$. The peaks labeled Z correspond to doubly protonated monomers: Val_n+2H^+. The Z peak with the highest mass (which is at a slightly lower mass than the $n = 10$ peak) corresponds to $Val_{20}+2H^+$. This shows that Val_{20} was generated in the synthesis. Its absence as a singly protonated ion in Figure 2 presumably results because it is large enough that electrospray produces it predominantly as a doubly charged ion. The series of peaks in Figure 2 labeled D correspond to doubly charged dimers, $Val_n+Val_m+2H^+$ with $n + m =$ odd. Doubly charged dimers with $n + m =$ even have the same mass-to-charge ratios as the singly charged monomers. Mass spectra for the other peptides studied in this work showed the same types of features as described above for Val_{20}.

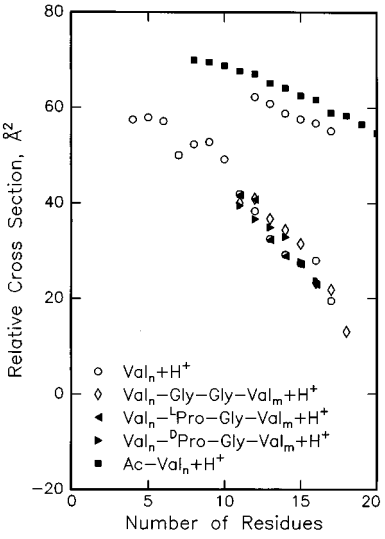

Figure 4. Relative cross-sections plotted against the number of residues. The relative cross-section scale (in Å^2) is given by $\Omega_{rel} = \Omega_{meas} - 19.02N - 11.91M$, where N is the number of valine and proline residues, and M is the number of glycine residues.

Figure 3 shows drift-time distributions (DTDs) recorded in the depletion mode for Val_n+H^+ with $n = 10-13$. The DTD measured for $Val_{10}+H^+$ shows a strong peak at ∼160 ms and two small, broader peaks around 140 ms. The small peaks are due to doubly charged dimers, $Val_n+Val_m+2H^+$ with $n + m =$ even, and other multimers which have the same m/z ratio as the singly charged monomers. DTDs measured with the mass spectrometer set to transmit ions with m/z ratios corresponding to $Val_n+Val_m+2H^+$ with $n + m =$ odd (the dimer peaks labeled D in Figure 2) show analogues of the small, broad peaks at shorter times (assigned to dimers) but no analogue of the narrow peak at longer time (assigned to the $Val_{10}+H^+$ monomer). With increasing peptide size, the dimer peaks (which move from ∼140 ms for $n = 10$ to ∼160 ms for $n = 13$) become broader and more difficult to discern from the baseline. The DTD for $n = 13$ shows two peaks due to the $Val_{13}+H^+$ monomer. The second peak, which first emerges around $n = 12$, is at a longer drift time than the first.

Cross-sections derived from the drift times for the Val_n+H^+ monomers are plotted in Figure 4 as the open circles. Cross-sections for Val_n+H^+, $n = 2-7$, were previously measured by Henderson et al.[53] In the region of overlap, their cross-sections were around 2% larger than ours. The relative cross-section scale used for the Val_n+H^+ data in Figure 4 is $\Omega_{rel} = \Omega_{meas} - 19.02N$, where 19.02 Å^2 is the cross-section per residue determined for an ideal polyvaline α-helix and N is the number of valine residues. Plotted in this way, α-helices have cross-sections that are independent of the number of residues, but random globules have cross-sections which decrease sharply with increasing peptide size. It is apparent from the drift-time distributions in Figure 3 that there are two distinct conformations present for the larger Val_n+H^+ peptides. The results for the conformation with the smaller relative cross-sections (the one that is present for all peptide sizes) are characteristic of random globules (the relative cross-sections decrease sharply with increasing peptide size). The results for this conformation are similar to the results that have been obtained for Gly_n+H^+ and Ala_n+H^+ peptides.[16] The other conformation, which first emerges around $n = 12$, is significantly less compact than a random globule. No analogue of this feature was observed for either Gly_n+H^+ or Ala_n+H^+.

(52) Shvartsburg, A. A.; Schatz, G. C.; Jarrold, M. F. *J. Chem. Phys.* **1998**, *108*, 2416−2423.
(53) Henderson, S. C.; Li, J.; Counterman, A. E.; Clemmer, D. E. *J. Phys. Chem. B* **1999**, *103*, 8780−8785.

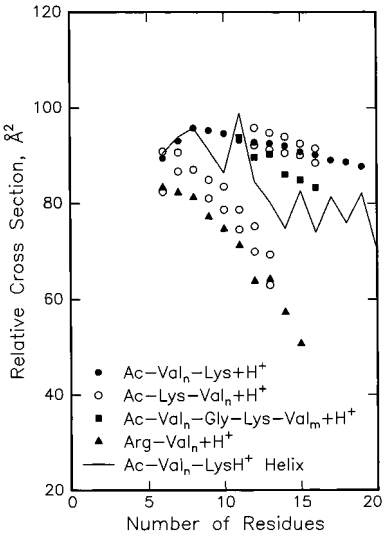

Figure 5. Relative cross-sections plotted against number of residues and calculated cross-sections for Ac-Val$_n$-LysH$^+$ helices (solid line). The relative cross-section scale (in Å^2) is given by $\Omega_{rel} = \Omega_{meas} - 19.02N - 11.91M$, where N is the number of valine and proline residues and M is the number of glycine residues.

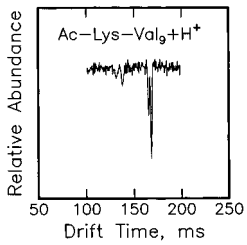

Figure 6. Drift-time distribution measured for Ac-Lys-Val$_9$+H$^+$.

Ac-Val$_n$-Lys+H$^+$ and Ac-Lys-Val$_n$+H$^+$ Peptides. Drift time distributions for Ac-Val$_n$-Lys+H$^+$ peptides with $n = 5-18$ show a single set of peaks. Relative cross-sections derived from the drift times are plotted in Figure 5 as filled circles (using the same scale as used for Val$_n$+H$^+$). The relative cross-sections are almost independent of the number of residues and close to the values expected for ideal α-helices (see below). The sharp decrease in the cross-sections that occurs for peptides with less than eight residues ($n < 7$) suggests that eight residues ($n = 7$) is the smallest stable Ac-Val$_n$-Lys+H$^+$ helix.

Drift time distributions measured for Ac-Lys-Val$_n$+H$^+$ $n = 5-10$ (except $n = 7$) consist of two closely spaced peaks. Only a single peak was observed for $n = 7$. Figure 6 shows the DTD measured for Ac-Lys-Val$_9$+H$^+$ having the two peaks at a drift time of around 170 ms. The broad peaks around 130−140 ms are due to dimers and other multimers. At $n = 11$, a second set of peaks emerges with longer drift times. These also consist of two closely spaced peaks. The two sets of peaks coexist up to around $n = 12$, then the peaks at longer times become dominant.

Relative cross-sections for the Ac-Lys-Val$_n$+H$^+$ peptides are plotted in Figure 5. The cross-sections for the first set of peaks decrease sharply with increasing peptide size, which is characteristic of random globules. For the second set of peaks, which first appear around $n = 11$, the relative cross-sections are similar to those obtained for the Ac-Val$_n$-Lys+H$^+$ peptides, in which the cross-sections were interpreted as indicating helical conformations. The appearance of the second set of peaks for Ac-Lys-Val$_n$+H$^+$ with $n = 11$ (12 residues) is similar to the results for Val$_n$+H$^+$ peptides in which a second peak, with a longer drift time, also emerges at around 12 residues. For the alanine and glycine analogues, Ac-Lys-Ala$_n$+H$^+$ and Ac-Lys-Gly$_n$+H$^+$, only a single set of peaks was observed, with relative mobilities characteristic of random globules.

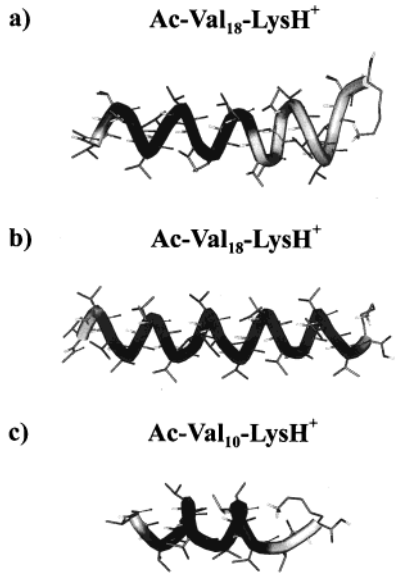

Figure 7. Final conformations from the MD simulations of helical Ac-Val$_n$-LysH$^+$ peptides: (a) final conformation from the Ac-Val$_{18}$-LysH$^+$ simulation that converted into a partial α-/partial π-helix; (b) final conformation from the Ac-Val$_{18}$-LysH$^+$ simulation that remained an α-helix for the first 960 ps; and (c) final conformation from the lowest energy simulation for Ac-Val$_{10}$-LysH$^+$ showing the partially unraveled C-terminus that is often observed for the smaller peptides. The images were produced using the WebLab viewer (Molecular Simulations Inc., San Diego, CA), and the α-helical regions have darker shading.

MD Simulations for Ac-Val$_n$-Lys+H$^+$ and Ac-Lys-Val$_n$+H$^+$ Peptides. For Ac-Val$_n$-Lys+H$^+$ and Ac-Lys-Val$_n$+H$^+$ we assume that the lysine amine is protonated (the N-terminus is blocked by acetylation). The lysine side chain has the highest solution pKa in these peptides, and proton affinities measured for individual amino acids and small peptides indicate that the lysine side chain should be the most basic site in vacuo.[54,55] In MD simulations for Ac-Val$_n$-LysH$^+$ started from an α-helix, the final conformation for $n > 12$ was usually a partial α-/partial π-helix, like that shown in Figure 7a for Ac-Val$_{18}$-LysH$^+$. This and subsequent images were obtained using the WebLab viewer (Molecular Simulations Inc., San Diego, CA). The α-helical regions have darker shading. A π-helix has i, $i + 5$ hydrogen bonds (4.4 residues per turn) while an α-helix has i, $i + 4$ hydrogen bonds (3.6 residues per turn). The amount of π-helix usually fluctuated between 1.5 and 3 turns. A π-helix may be favored at the C-terminus because it provides an extra carbonyl group to hydrogen bond to the protonated lysine, while the α-helix persists at the N-terminus presumably because it has one fewer dangling N−H group than the π-helix.

At least two simulations (960 ps at 300 K) with different initial conditions were performed for each Ac-Val$_n$-LysH$^+$ ($n = 5-19$) starting from an α-helix. The final conformations usually differed in how the protonated lysine side chain interacted with the C-terminus and in the relative amounts of α- and π-helices. Cross-sections derived from the lowest energy simulation for each peptide are plotted in Figure 5. The calculated cross-sections are below the measured ones for the

(54) Gorman, G. S.; Speir, J. P.; Turner, C. A.; Amster, I. J. *J. Am. Chem. Soc.* **1992**, *114*, 3986−3988.
(55) Wu, Z.; Fenselau, C. *Tetrahedron* **1993**, *49*, 9197−9206.

Table 1. Average Energies for Valine-, Alanine-, and Glycine-Based Peptides in Helical and Random Globular Conformations

peptide	energy,[a] kJ mol^{-1}		
	helix[b]	random globule[c]	helix−globule
Ac-Val_{19}-$LysH^+$	−2827	−2662 (−2678)[e]	−165
Ac-$LysH^+$-Val_{19}	−2500[d]	−2679	
Ac-Ala_{19}-$LysH^+$	−2819	−2690 (−2817)[f]	−129
Ac-$LysH^+$-Ala_{19}	*g*	−2717	
Ac-Gly_{19}-$LysH^+$	−2846	−2800	−46
Ac-$LysH^+$-Gly_{19}	*g*	−2811	

[a] Average potential energy from last 35 ps of the simulations. [b] Lowest energy simulation from five 300 K simulations started from an α-helix. [c] Lowest energy simulation from 10 simulated annealing runs started from an extended string. [d] In the five 300 K simulations run for Ac-$LysH^+$-Val_{19} starting from a helix, four remained largely helical, with average energies of −2492 to −2500 kJ mol^{-1}, and one collapsed to a partially helical globule, with an average energy of −2595 kJ mol^{-1}. The result in the Table is for the lowest energy helical conformation. [e] The two lowest energy simulated annealing runs for Ac-Val_{19}-$LysH^+$ were partially helical. The energy of the lowest energy one is shown in parentheses. [f] The five lowest energy simulated annealing runs for Ac-Ala_{19}-$LysH^+$ were either helical or partially helical. The energy for the lowest energy helix is shown in parentheses. [g] No helical conformations survived.

larger Ac-Val_n-Lys+H^+ peptides because the partial π-helices found in the simulations had smaller cross-sections than α-helices.

The transition from the initial α-helical structure to the partial π-conformation usually occurred early in the simulations. For example, the partial π-conformation in Figure 7a was established within the first 20 ps. In the other simulation performed for Ac-Val_{18}-$LysH^+$, the α-helix survived until the end of the simulation (960 ps). The final conformation from this simulation is shown in Figure 7b. The α-helix is 19 kJ mol^{-1} higher in energy than the partial π-helix in Figure 7a. In a second 960-ps simulation that followed the first, a partial π-helix began to form around 130 ps.

The average cross-section calculated for the Ac-Val_{18}-$LysH^+$ partial π-helix is 423 Å^2, and the cross-section calculated for the α-helix is 438 Å^2. These values bracket the measured value of 430 Å^2. The slight decrease in the measured relative cross-sections for Ac-Val_n-Lys+H^+ peptides with the number of residues (see Figure 5) suggests that their conformations are not entirely α-helical. However, the partial π-helices, which have the lowest energies in the simulations, have cross-sections which are smaller than the measured values. It is possible that the simulations slightly overestimate the stability of the partial π-helices, so that the average conformation lies between the partial π-helix and the α-helix shown in Figure 7. A conformation that fluctuates rapidly (on the experimental time scale) between these structures is also plausible.

Although the partial π-helix is the preferred conformation in the simulations for $n > 12$, for smaller peptides there are not enough turns to really establish this structure. A common structural motif for the smaller peptides is an α-helix, with the last turn at the C-terminus being partly unraveled. Like the C-terminus π-helix, this exposes an additional carbonyl group to hydrogen bond to the protonated lysine side chain. An example is shown in Figure 7c which shows the lowest energy conformation found for Ac-Val_{10}-$LysH^+$ in the simulations. This conformation has a cross-section that is slightly larger than the measured value (see Figure 5).

A number of simulations were performed for Ac-$LysH^+$-Val_{19} and Ac-Val_{19}-$LysH^+$ in order to compare the energies of the helices and random globules. Five 960-ps 300 K simulations were performed for each peptide starting from an α-helix. Average energies (from the last 35 ps) of the lowest energy simulations are shown in Table 1. For Ac-Val_{19}-$LysH^+$, in which the protonated lysine stabilizes the helix, the only notable difference between the simulations was the geometry at the C-terminus. In the five simulations run for Ac-$LysH^+$-Val_{19}, four remained helical and one collapsed to a partial-helix (smaller Ac-$LysH^+$-Val_n peptides, $n \leq 16$, and collapsed into random globules). According to the simulations, helical Ac-Val_{19}-$LysH^+$ is around 300 kJ mol^{-1} lower in energy than helical Ac-$LysH^+$-Val_{19} (see Table 1).

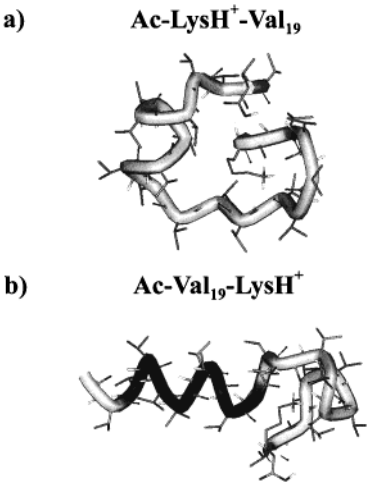

Figure 8. Final conformations from the lowest energy simulated annealing runs for (a) Ac-$LysH^+$-Val_{19} (b) Ac-Val_{19}-$LysH^+$. The images were produced using the WebLab viewer (Molecular Simulations Inc., San Diego, CA), and the α-helical region has darker shading.

Ac-$LysH^+$-Val_{19} and Ac-Val_{19}-$LysH^+$ random globules were prepared by starting the simulations from a fully extended all-trans geometry. Significantly lower energy random globules were prepared when using simulated annealing than were obtained when using collapse and quench at 300 K. Ten simulated annealing runs, with different starting conditions, were performed for Ac-$LysH^+$-Val_{19} and Ac-Val_{19}-$LysH^+$. The final conformation from the lowest energy simulated annealing run for Ac-$LysH^+$-Val_{19} is shown in Figure 8a. The random globule is close to 180 kJ mol^{-1} lower in energy than the helix for Ac-$LysH^+$-Val_{19} (see Table 1). The 10 simulated annealing runs yielded conformations with a relatively wide dispersion in energies (−2679 kJ mol^{-1} to −2580 kJ mol^{-1}) and geometries.

For Ac-Val_{19}-$LysH^+$, the two lowest energy simulated annealing runs were partially helical. In both cases, the N-terminus became helical, but the C-terminus wrapped around the protonated lysine side chain, allowing the backbone carbonyl groups to hydrogen bond to the protonated amine. This "self-solvation" shell formed before the helical section in the simulations, and did not reorganize into a helix, even though the partially helical conformation is much less stable than the full helix (see Table 1). The final conformation from the lowest energy Ac-Val_{19}-$LysH^+$ simulated annealing run is shown in Figure 8b.

In summary, Ac-Val_n-Lys+H^+ with $n > 7$ appeared to form partial π-helices. For Ac-Lys-Val_n+H^+ and Val_n+H^+ two distinct conformations were found. The conformation that occurred for the smaller peptides appeared to be a random globule. The less compact conformation that emerged around 12 residues for both peptides has yet to be explained. The second set of Ac-Lys-Val_n+H^+ peaks have relative mobilities that are coincident with those for the helical Ac-Val_n-Lys+H^+ peptides.

Table 2. Calculated Cross-Sections and Energies for Valine-Based β-Hairpins and Random Globules

peptide, charge site, and conformation	cross-section, Å^2	energy,[a] kJ mol^{-1}	rel energy, kJ mol^{-1}
$Val_{16}+H^+$ experiment	332, 361		
protonated at N-terminus amine			
simulated annealing, linear start[b]	338	−2113	0
β-hairpin at 300 K[c]	362	−2021	+92
Ac-Lys-$Val_{15}+H^+$ experiment	374, 377		
protonated at lysine side chain			
simulated annealing, linear start[b]	356	−2169	0
β-hairpin at 300 K[c]	371	−2126	+43
Val_7-Gly-Gly-Val_7+H^+ experiment	313		
protonated at N-terminus amine			
simulated annealing, linear start[b]	325	−2132[d]	0
β-hairpin at 300 K[c]	330	−2054	+78
Val_7-^{L}Pro-Gly-Val_7+H^+ experiment	320		
protonated at N-terminus amine			
simulated annealing, linear start[b]	325	−2043	0
β-hairpin at 300 K[c]	346	−1976	+67
Val_7-^{D}Pro-Gly-Val_7+H^+ experiment	321		
protonated at N-terminus amine			
simulated annealing, linear start[b]	331	−2077[d]	0
β-hairpin at 300 K[c]	341	−1988	+89
Ac-Val_7-Gly-Lys-Val_7+H^+ experiment	361		
protonated at lysine side chain			
simulated annealing, linear start[b]	346	−2175	0
β-hairpin at 300 K[c]	353	−2050	+125

[a] Average potential energy from last 35 ps of the simulations. [b] Lowest energy simulation from 10 simulated annealing runs which were started from a fully extended conformation. [c] Lowest energy simulation from 5 or 10 300 K simulations started from a β-hairpin. [d] Lowest energy geometry is a helix-turn. See Figure 10.

However, MD simulations for Ac-LysH^+-Val_n indicated that the helix is much higher in energy than the random globule. Furthermore, only random globules were observed for Ala_n+H^+ and Ac-Lys-Ala_n+H^+ peptides, and alanine has a much higher helix propensity than valine (in aqueous solution). Because valine is known to have a high propensity to form β-sheets, we should consider the possibility that the second set of peaks for Val_n+H^+ and Ac-Lys-Val_n+H^+ are due to β-hairpins.

Val_n+H^+ and Ac-Lys-Val_n+H^+ β-Hairpins. As a first test of the β-hairpin proposal, we performed molecular dynamics simulations for H^+Val_{16} ($Val_{16}+H^+$ protonated at the N-terminus[56]) and Ac-LysH^+-Val_{15} β-hairpins and random globules. The β-hairpin simulations were started with conformations near an ideal β-hairpin and were run for 960 ps at 300 K. Five β-hairpin simulations with different initial conditions were run for each peptide. Cross-sections and average energies for the lowest energy simulations are given in Table 2, and the final conformation from the lowest energy simulation for both peptides is shown in Figure 9. In all cases, a hairpin-like motif was retained to the end of the simulation. For $Val_{16}+H^+$, there is a short length of antiparallel β-sheet close to the turn, but it is disrupted at the ends of the hairpin by hydrogen bonds between backbone carbonyl groups and the protonated N-terminus (see Figure 9). The formation of the self-solvation shell around the protonated N-terminus presumably helps to stop the ends of the hairpin from fraying. The Ac-LysH^+-Val_{15} β-hairpin shows the same general features. Simulations were performed for random globules for comparison with the β-hairpins. Ten simulated annealing runs were performed for each peptide, starting from a fully extended all-trans geometry. Results for the lowest energy random globules are given in Table 2.

(56) Nair, H.; Wysocki, V. H. *Int. J. Mass Spectrom.* **1998**, *174*, 95−100.

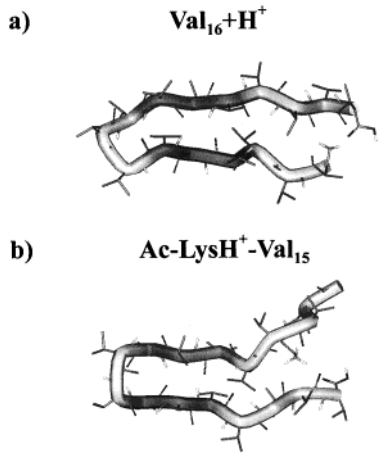

Figure 9. Final conformations from the lowest energy β-hairpin simulations for (a) $Val_{16}+H^+$ and (b) Ac-Lys-$Val_{15}+H^+$. The images were produced using the WebLab viewer (Molecular Simulations Inc., San Diego, CA), and the β-sheet regions have darker shading.

Cross-sections calculated for the H^+Val_{16} random globule and β-hairpin (338 Å^2 and 362 Å^2) are close to the cross-sections for the two features observed for $Val_{16}+H^+$ (332 Å^2 and 361 Å^2). For Ac-Lys-$Val_{15}+H^+$, the random globule was not observed. However, the cross-section calculated for Ac-LysH^+-Val_{15} β-hairpin (371 Å^2) was close to the cross-sections for the two closely spaced peaks observed for Ac-Lys-$Val_{15}+H^+$ (374 Å^2 and 377 Å^2). Thus, cross-sections calculated for β-hairpins were in reasonable agreement with the cross-sections for the more open conformations observed for both $Val_{16}+H^+$ and Ac-Lys-$Val_{15}+H^+$. However, for both H^+Val_{16} and Ac-LysH^+-Val_{15}, the simulations indicated that the β-hairpin was significantly higher in energy than the random globule (see Table 2). For H^+Val_{16}, the β-hairpin was calculated to be 92 kJ mol^{-1} less stable than the random globule, and for Ac-LysH^+-Val_{15}, the energy difference is 43 kJ mol^{-1}. For Ac-LysH^+-Val_{15}, simulated annealing runs started from a β-hairpin collapsed every time into a random globule. This is strong, but perhaps not conclusive, evidence that the β-hairpin structure is not stable for these peptides in vacuo. The simulations, which used an empirical force field, may be wrong.[57] The cross-sections calculated for the β-hairpins were sufficiently similar to the cross-sections for the helices that mobility measurements alone cannot be used to confirm the presence of the β-hairpin geometry. So to examine this issue more closely, we have used an approach based on designing better β-hairpins.

Designed β-Hairpins: Val_n-Xxx-Xxx-Val_n+H^+ Peptides. Although valine has a high propensity to form β-sheets, it is far from the best residue to have at the turn of a β-hairpin because it has such a bulky side chain.[58,59] Thus, one way to determine whether the less compact conformations observed for the Val_n+H^+ and Ac-Lys-Val_n+H^+ peptides are β-hairpins is to make some peptides with better β-turns. The following two-residue turns were considered:

1. Gly-Gly: this is the simplest two-residue turn. It occurs frequently in β-turns in proteins.[59] MD simulations of Val_5-Gly-Gly-Val_5-NH_2 have been performed in vacuo and in a simple model solvent.[60]

2. ^{D}Pro-Gly and ^{L}Pro-Gly: ^{D}Pro-Gly favors a Type II′ β-turn. Replacing ^{D}Pro with ^{L}Pro disrupts the β-hairpin.[61−63]

(57) Beachy, M. D.; Chasman, D.; Murphy, R. B.; Halgren, T. A.; Friesner, R. B. *J. Am. Chem. Soc.* **1997**, *119*, 5908−5920.
(58) Sibanda, B. L.; Thornton, J. M. *Nature* **1985**, *316*, 170−174.
(59) Gunasekaran, K.; Ramakrishnan, C.; Balaram, P. *Protein Eng.* **1997**, *10*, 1131−1141.

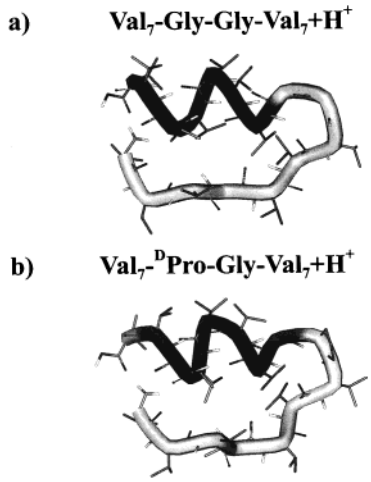

Figure 10. Final conformations from the lowest energy simulated annealing runs for (a) Val_7-Gly-Gly-Val_7+H^+ and (b) Val_7-^{D}Pro-Gly-Val_7+H^+. The images were produced using the WebLab viewer (Molecular Simulations Inc., San Diego, CA), and the α-helical regions have darker shading.

3. Gly-Lys: Gly-Lys was found as a two-residue turn in NMR studies of model β-hairpin peptides.[64] In an Ac-Val_n-Gly-Lys-Val_n peptide, the lysine side chain should be protonated, providing a test of whether the formation of a self-solvation shell at the end of the hairpin helps to stabilize it.

We synthesized the following peptides: Val_n-Gly-Gly-Val_n ($n = 5-8$), Val_n-^{L}Pro-Gly-Val_n ($n = 5-7$), Val_n-^{D}Pro-Gly-Val_n ($n = 5-7$), and Ac-Val_n-Gly-Lys-Val_n ($n = 5-7$). In each case a distribution of peptide sizes was evident in the mass spectrum. Cross-sections were determined for the synthetic target and the peptide with one fewer valine residue. The peptide with one fewer valine residue than the target is probably a mixture of peptides: Val_n-Gly-Gly-Val_{n-1}+H^+ and Val_{n-1}-Gly-Gly-Val_n+H^+. However, in all cases, only a single peak was observed in the DTDs.

Relative cross-sections for the Val_n-Gly-Gly-Val_m+H^+, Val_n-^{L}Pro-Gly-Val_m+H^+, and Val_n-^{D}Pro-Gly-Val_m+H^+ are plotted in Figure 4. The relative cross-section scale (in Å^2) used here is given by $\Omega_{rel} = \Omega_{meas} - 19.02N - 11.91M$, where N is the number of valine and proline residues, M is the number of glycine residues, and 19.02 and 11.91 are the cross-sections per residue for an ideal polyvaline and polyglycine α-helix, respectively. Because proline and valine have almost the same number of atoms and molecular weights, we assume that they make approximately the same contribution to the cross-sections. The relative cross-sections for Val_n-Gly-Gly-Val_m+H^+, Val_n-^{L}Pro-Gly-Val_m+H^+, and Val_n-^{D}Pro-Gly-Val_m+H^+ track the cross-sections for the more compact Val_n+H^+ conformations assigned to random globules (see Figure 4). This indicated that these peptides are not β-hairpins. Relative cross-sections for Ac-Val_n-Gly-Lys-Val_m+H^+ are plotted in Figure 5 (using the same scale). The relative cross-sections for these peptides track those determined for the less compact Ac-Lys-Val_n+H^+ conformations. So the Ac-Val_n-Gly-Lys-Val_m+H^+ peptides may be β-hairpins.

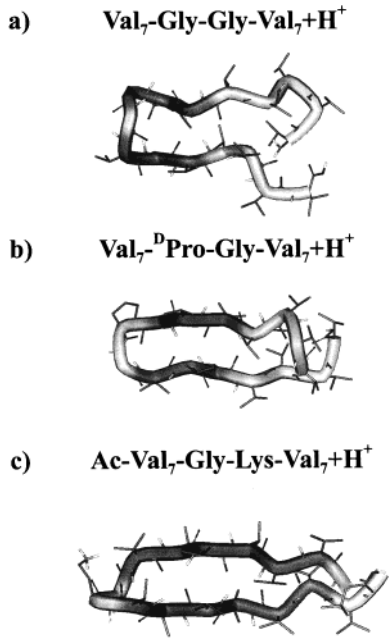

Figure 11. Final conformations from the lowest energy β-hairpin simulations for (a) Val_7-Gly-Gly-Val_7+H^+, (b) Val_7-^{D}Pro-Gly-Val_7+H^+, and (c) Ac-Val_7-Gly-Lys-Val_7+H^+. The images were produced using the WebLab viewer (Molecular Simulations Inc., San Diego, CA), and the β-sheet regions have darker shading.

MD Simulations for Val_n-Xxx-Xxx-Val_n+H^+ Peptides. Molecular dynamics simulations were performed for Val_7-Gly-Gly-Val_7+H^+, Val_7-^{L}Pro-Gly-Val_7+H^+, Val_7-^{D}Pro-Gly-Val_7+H^+, and Ac-Val_7-Gly-Lys-Val_7+H^+ for comparison to the experimental observations described above. The protonation site was assumed to be either the N-terminus or the lysine side chain. For each peptide, either 5 or 10 960-ps 300 K simulations were performed starting from a near ideal β-hairpin, and 10 simulated annealing runs were performed starting from a fully extended conformation. Most simulated annealing runs resulted in random globules. However, the lowest energy conformations found for both Val_7-Gly-Gly-Val_7+H^+ and Val_7-^{D}Pro-Gly-Val_7+H^+ were helix turns (see Figure 10). In these conformations, the turn is at the Gly-Gly or ^{D}Pro-Gly residues and the protonated N-terminus interacts with the C-terminus of the short helical section. Helix turns were not found in the simulations for Val_{16}+H^+ and Ac-LysH^+-Val_{15}, which suggests that they are promoted by the central turn residues. For Val_7-Gly-Gly-Val_7+H^+, the helix turn is 8 kJ mol^{-1} lower than the lowest energy random globule found in the simulated annealing runs, but for Val_7-^{D}Pro-Gly-Val_7+H^+, it is 19 kJ mol^{-1} lower.

Figure 11a,b shows the final conformations from the lowest energy β-hairpin simulations for Val_7-Gly-Gly-Val_7+H^+ and Val_7-^{D}Pro-Gly-Val_7+H^+. In both cases, there is a short stretch of antiparallel β-sheet near the turn, and the end of the hairpin is disrupted by hydrogen bonds between the N-terminus and the backbone carbonyl groups. Compared to Val_{16}+H^+ and Ac-Lys-Val_{15}+H^+ in Figure 9, incorporation of better β-turns does not seem to have improved the β-hairpins. Figure 11c shows the final conformation from the lowest energy simulation for Ac-Val_7-Gly-Lys-Val_7+H^+. Moving the protonation site from the N-terminus has led to substantially more antiparallel β-sheet, but hydrogen bonding to the protonated lysine side chain has distorted the turn region.

Calculated cross-sections and energies from the lowest energy β-hairpin and simulated annealing runs for Val_7-Gly-Gly-Val_7+H^+, Val_7-^{L}Pro-Gly-Val_7+H^+, Val_7-^{D}Pro-Gly-Val_7+H^+,

(60) Sung, S.-S. *Biophys. J.* **1999**, *76*, 164−175.
(61) Haque, T. S.; Little, J. C.; Gellman, S. H. *J. Am. Chem. Soc.* **1996**, *118*, 6975−6985.
(62) Karle, I. L.; Awasthi, S. K.; Balaram, P. *Proc. Natl. Acad. Sci. U.S.A.* **1996**, *93*, 8189−8193.
(63) Schenck, H. L.; Gellman, S. H. *J. Am. Chem. Soc.* **1998**, *120*, 4869−4870.
(64) de Alba, E.; Jiménez, M. A.; Rico, M. *J. Am. Chem. Soc.* **1997**, *119*, 175−183.

Table 3. Relative Proton Affinities[a] of the Different Protonation Sites of a Gly_3 Peptide, According to Quantum Chemical Calculations by Zhang et al.[65]

protonation site	rel proton affinity kJ mol^{-1}
N-terminus amine (N1)	0
amide CO group nearest to N-terminus (O1)	21
amide CO group furthest from N-terminus (O2)	52
carboxyl CO group (O3)	77
amide NH group nearest to N-terminus (N2)	88
amide NH group furthest from N-terminus (N3)	104

[a] Calculations were performed at the 3-21G//6-31G* level.

and Ac-Val_7-Gly-Lys-Val_7+H^+ are shown in Table 2. For Val_7-Gly-Gly-Val_7+H^+, Val_7-^{L}Pro-Gly-Val_7+H^+, and Val_7-^{D}Pro-Gly-Val_7+H^+, the cross-sections calculated for the β-hairpins were significantly larger than the measured cross-sections. Cross-sections from the lowest energy simulated annealing runs for these peptides, which are random globules or helix-turns, were slightly larger than the measured ones. For Ac-Val_7-Gly-Lys-Val_7+H^+, the calculated cross-section for the β-hairpin was close to the measured cross-section, leaving open the possibility that the less-compact conformation seen for this peptide (see Figure 5) is a β-hairpin.

It is apparent from Table 2 that the average energies of the β-hairpins are significantly higher than those of the conformations which were derived from simulated annealing, including Ac-Val_7-Gly-Lys-Val_7+H^+, in which the energy difference was actually the largest despite the fact that this peptide has the most extensive region of antiparallel β-sheet. This explains why β-hairpins were not observed in the experiments for Val_n-Gly-Gly-Val_m+H^+, Val_n-^{L}Pro-Gly-Val_m+H^+, and Val_n-^{D}Pro-Gly-Val_m+H^+: they are not energetically favorable. In view of the large energy difference between the β-hairpin and the random globule for Ac-Val_n-Gly-Lys-Val_m+H^+, it seems likely that the less-compact conformation observed for this peptide is not a β-hairpin either. So the nature of the less compact conformations observed for Val_n+H^+, Ac-Lys-Val_n+H^+, and Ac-Val_n-Gly-Lys-Val_m+H^+ still needs to be explained.

Are Val_n+H^+, Ac-Lys-Val_n+H^+, and Ac-Val_n-Gly-Lys-Val_m+H^+ Helical. Comparison of the peptides that have the less compact conformations (Val_n+H^+, Ac-Lys-Val_n+H^+, and Ac-Val_n-Gly-Lys-Val_m+H^+) to those that do not (Val_n-Gly-Gly-Val_m+H^+, Val_n-^{L}Pro-Gly-Val_m+H^+, and Val_n-^{D}Pro-Gly-Val_m+H^+) reveals that the difference among them is the presence of helix-breaking residues in the center of the peptides that do not form the less-compact conformation. This leads us to reconsider the possibility that the less-compact conformations are helical.

One way for Val_n+H^+ and Ac-Lys-Val_n+H^+ peptides to become helical is for the proton to be located at the C-terminus instead of the N-terminus or on the lysine side chain. Table 3 shows relative proton affinities obtained from quantum chemical calculations for protonation at different sites on Gly_3.[65] According to these calculations, the N-terminus has the highest proton affinity, and protonation at the amide CO furthest from the N-terminus is less favorable by 52 kJ mol^{-1}. It is energetically feasible for the proton to relocate if the free energy gained by transforming from a random globule to a helix is greater than the difference in the proton affinities of the two sites.[66] It is relatively easy to design peptides to test for this possibility.

Table 4. Proton Affinities of Relevant Amino Acids and Other Simple Molecules from the Compilation of Hunter and Lias[67]

molecule	proton affinity kJ mol^{-1}
valine	911
lysine	996
$CH_3CH_2CH_2NH_2$ (lysine side chain analogue)	918
arginine	1051
guanidine (arginine side chain analogue)	986

Table 4 shows a summary of the proton affinities of the relevant amino acids and side chain analogues.[67] Lysine has a much larger proton affinity than valine. However, the large proton affinity of lysine is mainly due to favorable intramolecular interactions (protonated lysine adopts a cyclic geometry where the proton interacts with the side-chain amine and the N-terminus amine).[68] The proton affinity of propylamine (an analogue of the lysine side chain) is close to that of valine. Arginine is more basic than lysine, because it contains the strongly basic guanidine group. According to the data in Table 4, the proton affinity of the arginine side chain is 65−75 kJ mol^{-1} larger than the valine N-terminus and the lysine side chain. Thus, arginine at the N-terminus of a valine peptide should ensure that the proton remains at the N-terminus. Therefore, $ArgH^+$-Val_n should not form helices. On the other hand, acetylating the N-terminus of polyvaline should decrease the cost of protonating the C-terminus, and so helices should form for smaller Ac-Val_n+H^+ peptides than for Val_n+H^+.

Ac-Val_n+H^+ and Arg-Val_n+H^+. Drift-time distributions measured for both Arg-Val_n+H^+ and Ac-Val_n+H^+ showed a single set of peaks due to the monomer. Relative cross-sections for the Ac-Val_n+H^+ peptides are shown in Figure 4. The relative cross-section scale used for the Ac-Val_n+H^+ data is $\Omega_{rel} = \Omega_{meas} - 19.02N$, where N is the number of valine residues. The relative cross-sections for the larger Ac-Val_n+H^+ peptides lie slightly above the data for the less-compact Val_n+H^+ conformation. This suggests that the Ac-Val_n+H^+ peptides adopt the same (presumably helical) conformation as the larger Val_n+H^+ peptides. The small difference between the relative cross-sections of Ac-Val_n+H^+ and Val_n+H^+ results because the acetyl group makes the Ac-Val_n+H^+ peptides slightly larger than their Val_n+H^+ analogues. For Ac-Val_n+H^+, there is no analogue of the more compact (random globule) conformation observed for the smaller Val_n+H^+ peptides. Instead, the less compact (presumably helical) conformation persists to smaller Ac-Val_n+H^+ peptides, as predicted.

Relative cross-sections for Arg-Val_n+H^+ are shown in Figure 5. The relative cross-section scale used for the Arg-Val_n+H^+ data is $\Omega_{rel} = \Omega_{meas} - 19.02N$, where N is the number of valine residues. The results for Arg-Val_n+H^+ track the data for the compact form (random globule) of the Ac-Lys-Val_n+H^+ peptides. (We assume that lysine and arginine make approximately the same contribution to the cross-section). No analogue of the less compact, presumably helical, conformation was observed. Thus, Arg-Val_n+H^+ is random globules, as predicted. These

(65) Zhang, K.; Cassady, C. J.; Chung-Phillips, A. *J. Am. Chem. Soc.* **1994**, *116*, 11512−11521.

(66) The basic notion here is different from the "mobile proton" model that has been used to explain some features of the fragmentation behavior of peptide ions (Dongre, A. R.; Jones, J. L.; Somogyi, Á.; Wysocki, V. H. *J. Am. Chem. Soc.* **1996**, 8365−8374). In the "mobile proton" model there is an energy penalty associated with mobilizing the proton; here, the proton relocates because a conformational change makes it energetically favorable.

(67) Hunter, E. P.; Lias, S. G. In *NIST Chemistry WebBook*: NIST Standard Reference Database Number 69; Mallard, W. G., Linstrom, P. J., Eds.; National Institute of Standards and Technology: Gaithersburg, MD, 2000 (http://webbook.nist.gov).

(68) Bliznyuk, A. A.; Schaefer, H. F.; Amster, I. J. *J. Am. Chem. Soc.* **1993**, *115*, 5149−5154.

Table 5. Calculated Cross-Sections and Energies for α-Helices and Random Globules Generated by Protonating the C-Terminus

peptide, charge site, and conformation	structure[a]	cross-section, Å^2	energy,[b] kJ mol^{-1}	rel energy, kJ mol^{-1}
$Val_{16}+H^+$ experiment		332, 361		
protonated at C-terminus amide CO				
simulated annealing, linear start[c]	helix (4/10)	353	−2877	−131
	glob (2/10)	(348)	(−2670)	(+76)
α-helix at 300 K	helix (5/5)	374[e]	−2871	−125
simulated annealing, random globule[d]	glob (10)	347	−2746	0
protonated at C-terminus COOH				
simulated annealing, linear start[c]	helix (2/10)	351	−2630	−101
	glob (6/10)	(344)	(−2518)	(+11)
α-helix at 300 K	helix (5/5)	349	−2643	−114
simulated annealing, random globule[d]	glob (11)	336	−2529	0
Ac-$Val_{16}+H^+$ experiment		366		
protonated at C-terminus amide CO				
simulated annealing, linear start[c]	helix (4/10)	366	−2940	−59
	glob (2/10)	(353)	(−2833)	(+48)
α-helix at 300 K	helix (5/5)	381[e]	−3007	−126
simulated annealing, random globule[d]	glob (12)	343	−2881	0
Ac-Lys-$Val_{15}+H^+$ experiment		374, 377		
protonated at C-terminus amide CO				
simulated annealing, linear start[c]	helix (3/10)	368	−2996	−108
	glob (1/10)	(353)	(−2860)	(+28)
α-helix at 300 K	helix(5/5)	390[e]	−2999	−111
simulated annealing, random globule[d]	glob (12)	340	−2888	0

[a] Conformation at the end of the simulation is defined as either largely helical (helix), partially helical (p/helix), or random globule (glob). The number in parentheses gives the number of simulations assigned to a particular group. [b] Average potential energy from last 35 ps of the simulations. [c] Lowest energy simulated annealing run was helical. Results for lowest energy globule shown in parentheses. [d] Ten 100-ps simulations were performed at 600 K, and the random globules were selected and used as starting points for a simulated annealing schedule of 240 ps at 500 K, 240 ps at 400 K, and 480 ps at 300 K. Some globules converted into helices or partial helices during the simulated annealing runs. This procedure was repeated until enough random globules were generated. [e] Lowest energy helix is mainly an α-helix.

experimental results support the idea that the less compact conformations observed for the larger Val_n+H^+ and Ac-Lys-Val_n+H^+ peptides are helical, with the proton located at the C-terminus.

MD Simulations for $Val_{16}+H^+$, Ac-$Val_{16}+H^+$, and Ac-Lys-$Val_{15}+H^+$ Helices. To further examine the helical states for these peptides, a series of molecular dynamics simulations were performed for $Val_{16}+H^+$, Ac-$Val_{16}+H^+$, and Ac-Lys-$Val_{15}+H^+$ protonated at the amide CO nearest the C-terminus. We also performed simulations for $Val_{16}+H^+$ protonated at the carboxyl CO. According to the information shown in Table 3, the carboxyl CO is the second most favorable protonation site near the C-terminus. The results are summarized in Table 5. In each case we performed 5 960-ps 300 K simulations starting from an α-helix and 10 simulated annealing runs starting from a fully extended all-trans geometry. The majority of the simulated annealing runs generated either helices or partially helical conformations (see Table 5).

Because so few of the simulated annealing runs led to random globules, we modified our procedure to generate more of them. A series of 10 100-ps simulations were performed at 600 K, and the random globules were selected and run for 240 ps at 500 and 400 K and then 480 ps at 300 K. Some of the random globules became helical or partially helical during the rest of the simulated annealing run. This procedure was repeated several times to yield 10−12 random globules. The cross-sections and average energies for the random globule with the lowest final energy are shown in Table 5.

The final conformations from the simulations that lead to the lowest energy helix for $Val_{16}+H^+$ protonated at the amide CO and at the carboxyl CO are shown in Figure 12a,b, respectively. In both cases, there is a partial π-helix at the C-terminus, and the protonated group is twisted around so that it can interact with the dangling CO groups at the end of the helix. The cross-sections which were calculated for the lowest energy $Val_{16}+H^+$ helices are slightly smaller than the measured values (see Table 5). The lowest energy helices for Ac-$Val_{16}+H^+$ and Ac-Lys-$Val_{15}+H^+$ that are protonated at the amide CO are similar to the $Val_{16}+H^+$ helix shown in Figure 12a. For Ac-$Val_{16}+H^+$, the helices formed by simulated annealing are significantly higher in energy than those produced in the 960-ps 300 K simulations started from an α-helix (see Table 5). The helices formed by simulated annealing have their C-termini distorted to form a self-solvation shell around the protonated CO group.

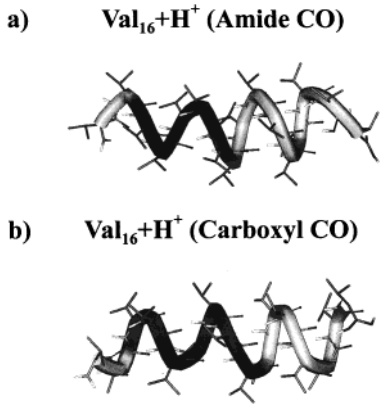

Figure 12. Final conformations from the simulation (simulated annealing or 300 K MD simulation) that led to the lowest energy helix for (a) $Val_{16}+H^+$ protonated at the amide CO nearest the C-terminus and (b) $Val_{16}+H^+$ protonated at the carboxyl CO. The images were produced using the WebLab viewer (Molecular Simulations Inc., San Diego, CA), and the α-helical regions have darker shading.

It is not possible to directly compare the energies obtained from the simulations for different protonation sites. However, relative energies, the difference between the lowest energy helix and the lowest energy random globule, can be compared. According to the results shown in Table 5, the relative energy for $Val_{16}+H^+$ protonated at the amide CO (−131 kJ mol^{-1}) is

Table 6. Calculated Cross-Sections and Energies for α-Helices and Random Globules Generated by Protonating the C-terminus of Val_7-Xxx-Xxx-Val_7+H^+ Peptides

peptide, charge site, and conformation	structure[a]	cross-section, Å^2	energy,[b] kJ mol^{-1}	rel energy, kJ mol^{-1}
Val_7-Gly-Gly-Val_7+H^+ experiment		313		
protonated at C-terminus amide CO				
simulated annealing, linear start[c]	helix (2/10)	353	−2823	−50
	glob (7/10)	(332)	(−2773)	0
α-helix at 300 K	helix (5/5)	364[e]	−2866	−93
simulated annealing, helical start	helix (5/5)	347	−2866	−93
Val_7-^{L}Pro-Gly-Val_7+H^+ experiment		320		
protonated at C-terminus amide CO				
simulated annealing, linear start	glob (10/10)	332	−2688	0
α-helix at 300 K	helix (5/5)	336[f]	−2736	−48
simulated annealing, helical start	helix (5/5)	347[f]	−2759	−71
protonated at C-terminus COOH				
simulated annealing, linear start	glob (10/10)	324	−2470	0
α-helix at 300 K	helix (5/5)	338	−2505	−35
simulated annealing, helical start	helix (5/5)	340[f]	−2525	−55
Ac-Val_7-Gly-Lys-Val_7+H^+ experiment		361		
protonated at C-terminus amide CO				
simulated annealing, linear start[c]	helix (4/10)	380	−2952	−71
	glob (4/10)	(352)	(−2865)	+16
α-helix at 300 K	helix (5/5)	352[f]	−2987	−106
simulated annealing, helical start	helix (5/5)	364	−3006	−125
simulated annealing, random globule[d]	glob (8)	344	−2881	0
protonated at lysine side chain				
simulated annealing, linear start	glob (10/10)	346	−2175	0
α-helix at 300 K	helix (5/5)	376	−2217	−42

[a] Conformation at the end of the simulation is defined as either largely helical (helix), partially helical (p/helix), or random globule (glob). The number in parentheses gives the number of simulations assigned to a particular group. [b] Average potential energy from last 35 ps of the simulations. [c] Lowest energy simulated annealing run was helical. Results for lowest energy globule shown in parentheses. [d] Ten 100-ps simulations were performed at 600 K, and the random globules were selected and used as starting points for a simulated annealing schedule of 240 ps at 500 K, 240 ps at 400 K, and 480 ps at 300 K. Some globules converted into helices or partial helices during the simulated annealing runs. This procedure was repeated until enough random globules were generated. [e] Lowest energy helix is mainly an α-helix. [f] Lowest energy helix is mainly a π-helix.

slightly larger than the relative energy for protonation at the carboxyl CO (−114 kJ mol^{-1}). Small differences between the relative energies are probably not significant because our simulated annealing runs probably did not find the lowest energy conformations. The relative energies do not include the difference between the proton affinities of the protonation sites. This favors protonation at the amide CO nearest the C-terminus (see Table 3). For Ac-Val_{16}+H^+ and Ac-Lys-Val_{15}+H^+ protonated at the amide CO, the energy differences are −126 kJ mol^{-1} and −111 kJ mol^{-1}, respectively. The relative energies found here are similar to the energy difference between the Ac-Val_{15}-LysH^+ helix and the Ac-LysH^+-Val_{15} random globule (−108 kJ mol^{-1}).

The MD simulations described above indicated that the helical conformation is >100 kJ mol^{-1} lower in energy than the random globule for Val_{16}+H^+, Ac-Val_{16}+H^+, and Ac-Lys-Val_{15}+H^+ protonated at the amide CO. This is much larger than the energy penalty of around 52 kJ mol^{-1} (from Table 3) associated with protonating the amide CO nearest the C-terminus instead of the N-terminus or the lysine side chain nearest the N-terminus. Thus these results suggest that it is energetically favorable to protonate the C-terminus and form a helix in these peptides.

The Val_n-Xxx-Xxx-Val_n+H^+ Peptides Revisited. Of the peptides designed to be β-hairpins, Val_7-Gly-Gly-Val_7+H^+, Val_7-^{L}Pro-Gly-Val_7+H^+, and Val_7-^{D}Pro-Gly-Val_7+H^+ appear to be random globules. Protonation at the C-terminus of these peptides should also promote helix formation. The fact that helices are not formed with these peptides must be due to the presence of glycine and proline. Both glycine and proline are considered to be helix-breakers in solution.[1] A series of MD simulations were performed to examine how the glycine and proline disrupt helix formation.

Ten standard simulated annealing runs, started from a fully extended all-trans geometry, and five 960-ps 300 K simulations, started from an α-helix, were performed for Val_7-Gly-Gly-Val_7+H^+ and Val_7-^{L}Pro-Gly-Val_7+H^+ protonated at the amide CO nearest the C-terminus and for Val_7-^{L}Pro-Gly-Val_7+H^+ protonated at the carboxyl CO. We also performed five standard simulated annealing runs, started from an α-helix, for each peptide. These remained helical, although a considerable amount of fraying occurred at the N-terminus at the higher temperatures. The results for the lowest energy simulations are summarized in Table 6.

For Val_7-Gly-Gly-Val_7+H^+, the lowest energy helix was 93 kJ mol^{-1} more stable than the lowest energy random globule. This energy difference was less than that found for Ac-Val_{16}+H^+ and Val_{16}+H^+ protonated at the amide CO. There was little difference between the results for Val_7-^{L}Pro-Gly-Val_7+H^+ protonated at the amide CO and at the carboxyl CO. The energy difference between the random globule and the helix was relatively small and less than that for Val_7-Gly-Gly-Val_7+H^+. Proline is known to disrupt the intra-helical hydrogen bonding framework. This was apparent in the simulations, and it was responsible for destabilizing the helices that incorporated proline. For both protonation sites the lowest energy helices were mainly π-helices. The final conformation from the lowest energy simulation for helical Val_7-^{L}Pro-Gly-Val_7+H^+ (protonated at the amide CO) is shown in Figure 13a.

For Ac-Val_7-Gly-Lys-Val_7+H^+, the lowest energy helix is a partial π-helix similar to that shown in Figure 12a for Val_{16}+H^+. Because relatively few of the standard simulated annealing runs led to random globules, some additional runs were performed in order for this peptide to generate more random globules. The energy difference between the random globule and the helix

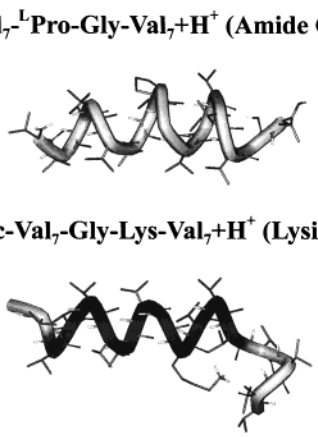

Figure 13. Final conformations from (a) the lowest energy helix found for Val_7-^{L}Pro-Gly-Val_7+H^+ protonated at the amide CO nearest the C-terminus and (b) the lowest energy 300 K MD simulation for helical Ac-Val_7-Gly-Lys-Val_7+H^+ protonated at the lysine side chain. The images were produced using the WebLab viewer (Molecular Simulations Inc., San Diego, CA), and the α-helical regions have darker shading.

for Ac-Val_7-Gly-Lys-Val_7+H^+ (125 kJ mol^{-1}) is similar to the difference for Ac-Val_{16}+H^+ and Val_{16}+H^+.

For Ac-Val_7-Gly-Lys-Val_7+H^+, it may be possible to form a helix with the central lysine being protonated. Some MD simulations were performed to examine this possibility. All of the 960-ps 300 K simulations that started from an α-helix resulted in final conformations in which the N-terminus remained helical and the C-terminus was distorted to provide a self-solvation shell around the protonated lysine side chain. The final conformation from the lowest energy helical simulation is shown in Figure 13b. The energy difference between the random globule and the helix for Ac-Val_7-Gly-Lys-Val_7+H^+ protonated at the lysine side chain is only 42 kJ mol^{-1}, which is considerably less than that which was found when the amide CO nearest the C-terminus was protonated. The small difference resulted because formation of the self-solvation shell around the protonated lysine side chain disrupts the helix at the C-terminus.

Discussion

Partial π-Helix Formation. In many of the molecular dynamics simulations of the valine-based peptides studied here, the favored helical conformation was a partial α-/partial π-helix with the π-helix portion located at the C-terminus. The observation of π-helices in peptides and proteins has been limited.[69,70] In the present case, the partial π-helix was preferred presumably because it provided an additional backbone carbonyl group to interact with the protonated group at the C-terminus. A similar partial α-/partial π-helix was found to be prominent in MD simulations of glycine-based peptides.[27] However, the experimental results indicate that both Ac-$LysH^+$-Gly_n and Ac-Gly_n-$LysH^+$ form random globules. For the valine-based peptides, the slight decrease in the measured relative cross-sections with peptide size and comparison of the measured and calculated cross-sections support the presence of a small π-helix component.

The partial α-/partial π-helix motif was not found to be prominent in MD simulations of alanine-based peptides.[21] In MD simulations of blocked (Ala-Ala-Xxx-Ala-Ala) peptides with Xxx = Gln, Asn, Glu, Asp, Arg, and Lys, it was found that side-chain interactions could promote π-helix formation.[71] It is possible that the bulky side chains in the valine-based peptides are a factor in promoting partial π-helix formation, and this also may explain why the partial π-helix is less favored in the alanine-based peptides.

Table 7. Values of ΔG, ΔH, and $-T\Delta S$ at 300 K for Some Small, Neutral Peptides[a]

peptide	ΔG, kJ mol^{-1}	ΔH, kJ mol^{-1}	$-T\Delta S$, kJ mol^{-1}
Gly_{10}	10	−1	11
Val_{10}	0	−13	13
Ala_{10}	−13	−32	19
Ala_{15}	−39	−99	59
Ala_{20}	−72	−187	115

[a] Calculated by multicanonical Monte Carlo method by Okamoto and Hansmann[30]

***β*-Hairpin Formation in Valine-Based Peptides.** It is apparent from the experimental results presented here that valine-based peptides do not form β-hairpins. The MD simulations indicate that the β-hairpin is energetically unfavorable. While we do not have an estimate of $T\Delta S$ for hairpin formation, entropy must oppose hairpin formation, and so the free energies for hairpin formation are even more unfavorable than the energies derived from the MD simulations. These results are consistent with previous MD simulations performed by Sung.[60]

An ideal valine-based β-hairpin with around 16 residues has a smaller network of hydrogen bonds than does a helix with the same number of residues, and this is probably a factor in accounting for why the β-hairpin is significantly higher in energy than the helix is for the peptides studied here. It still may be possible to stabilize the β-hairpin geometry in vacuo through side-chain interactions. It has been suggested that the de novo β-hairpin peptide of Ramirez-Alvarado and collaborators[72] (RGITVNGKTYGR) retains this geometry in the vapor phase.[73]

The Entropy Cost of Helix Formation. As alluded to above, there is an entropy cost associated with fixing peptides into particular conformations such as helices or hairpins. This entropy cost is not easy to estimate. Table 7 summarizes enthalpy and entropy changes calculated by Okamoto and Hansmann for the helix to coil transition in a number of small peptides in the gas phase.[30] The calculations were performed using multicanonical Monte Carlo. From these results, we estimate $-T\Delta S$ for the helix-to-random globule (or -random coil) transition for Val_{16} to be ∼48 kJ mol^{-1} at 300 K.

The free energy change for helix formation in the peptides considered here can be estimated by making the following three assumptions: 1. The energy difference between the helical conformation and the random globule, determined from the MD simulations, is equivalent to an enthalpy difference. 2. $-T\Delta S$ for helix formation at 300 K is 48 kJ mol^{-1} for all of the 16 residue peptides considered here. 3. The energy cost for protonating the amide CO nearest the C-terminus and carboxyl CO are 52 kJ mol^{-1} and 77 kJ mol^{-1}, respectively, unless the amide CO is the lowest energy protonation site available.

Estimated free energy changes for helix formation are given in Table 8. The peptides studied here fall into three groups: strong helix-formers, weak helix-formers, and nonhelical. In the strong helix-formers, Ac-Lys-Val_{15}+H^+ (protonated at the lysine amine) and Ac-Val_{16}+H^+ (protonated at the amide CO), there

(69) Creighton, T. E. *Proteins*; W. H. Freeman and Co.: New York, 1993.
(70) Rohl, C. A.; Doig, A. J. *Protein Sci.* **1996**, *5*, 1687−1696.
(71) Shirley, W. A.; Brooks, C. L. *Proteins: Struct. Funct. Genet.* **1997**, *28*, 59−71.
(72) Ramirez-Alvarado, M.; Blanco, F. J.; Serrano, L. *Nat. Struct. Biol.* **1996**, *3*, 604−612.
(73) Li, A.; Feneslau, C.; Kaltashov, I. A. *Proteins: Struct. Funct. Genet. Suppl.* **1998**, *2*, 22−27.

Table 8. Free Energies of Helix Formation Estimated for the Valine-Based Peptides Studied Here

peptide (protonation site)	ΔE from MD,[a] kJ mol^{-1}	$\Delta E+\Delta PA$,[b] kJ mol^{-1}	ΔG helix,[c] kJ mol^{-1}	helix formed[d]
		Strong Helix Formers		
Ac-Val_{15}-Lys+H^+ (lysine)[e]	−108	−108	−60	yes
Ac-Val_{16}+H^+ (amide CO)	−126	−126	−78	yes
		Weak Helix Formers		
Val_{16}+H^+ (amide CO)	−131	−79	−31	yes
Val_{16}+H^+ (COOH)	−114	−37	+11	yes
Ac-Lys-Val_{15}+H^+ (amide CO)	−111	−59	−11	yes
Ac-Val_7-Gly-Lys-Val_7+H^+ (amide CO)	−125	−73	−25	yes
Ac-Val_7-Gly-Lys-Val_7+H^+ (lysine)	−42	−42	+6	yes
		Nonhelical		
Val_7-Gly-Gly-Val_7+H^+ (amide CO)	−93	−41	+7	no
Val_7-^{L}Pro-Gly-Val_7+H^+ (amide CO)	−71	−19	+29	no
Val_7-^{L}Pro-Gly-Val_7+H^+ (COOH)	−55	+22	+70	no

[a] Energy difference in MD simulations between lowest energy helix and lowest energy random globule. [b] Calculated assuming that the energy cost for protonating the amide CO nearest the C-terminus is 52 kJ mol^{-1}, unless it is the lowest energy protonation site available, and that the energy cost for protonating the carboxyl CO is 77 kJ mol^{-1}. [c] Calculated assuming $T\Delta S$ is −48 kJ mol^{-1} for all peptides. [d] Whether or not the helix is observed in the experiments. [e] Energy difference between the Ac-Val_{15}-LysH^+ helix and the Ac-LysH^+-Val_{15} random globule.

is no energy penalty for locating the proton at the C-terminus. The estimated free energy change for helix formation in these peptides is ∼−60 to −80 kJ mol^{-1}. The experimental results indicated that these peptides are helical, as predicted.

In the weak helix-formers, Val_{16}+H^+, Ac-Lys-Val_{15}+H^+, and Val_7-Gly-Lys-Val_7+H^+ (all protonated at the amide CO), there is an energy penalty (assumed to be 52 kJ mol^{-1}) for protonating the C-terminus. For these peptides, the free energy change for helix formation is small and negative, between −11 and −31 kJ mol^{-1}. The experimental results indicated that they are helical, as predicted. For Val_{16}+H^+, protonation at the carboxyl CO leads to a positive free energy change for helix formation because of the larger energy penalty for protonating this site. The free energy change for helix formation is also positive for Ac-Val_7-Gly-Lys-Val_7+H^+ protonated at the lysine side chain. Here the positive free energy change results because the energy difference between the helix and the random globule is quite small (the protonated lysine side chain disrupts the C-terminus of the helix).

In the nonhelical peptides, Val_7-Gly-Gly-Val_7+H^+ and Val_7-^{L}Pro-Gly-Val_7+H^+, both of which are protonated at the amide CO nearest the C-terminus, there is an energy penalty, which is assumed to be 52 kJ mol^{-1}, for locating the proton at the C-terminus. Furthermore, incorporation of the Gly-Gly and Pro-Gly residues causes a significant decrease in the stability of the helix relative to the random globule. This leads to a positive free energy change for helix formation. The experimental results indicated that these peptides are random globules, as predicted. Note that the energy penalty for introducing Pro-Gly into the center of the helix appears to be larger than that for introducing Gly-Gly, although both ultimately disrupt helix formation. As noted above, proline disrupts the intra-helical hydrogen bonding framework. The overall agreement between the predicted free energy changes for helix formation and the experimental conformations is remarkably good (see Table 8). The CHARMM force field employed in the simulations is apparently providing a reasonably good estimate of the relative energies of the different conformations.

Valine Has a Higher Helix Propensity Than Alanine. The free energies of helix formation for the weak helix-formers are small and negative (see Table 8). The alanine analogues of these peptides, Ala_{16}+H^+ and Ac-Lys-Ala_{15}+H^+, were not found to form helices (measurements were not performed for Ala_7-Gly-Lys-Ala_7+H^+), suggesting that the free energies for helix formation in the alanine analogues are positive. This suggests that valine has a higher helix propensity than does alanine in vacuo. According to MD simulations, the energy difference between the helix and the random globule for Ac-Val_{19}-LysH^+ is −165 kJ mol^{-1}. We performed a similar set of simulations for the alanine and glycine analogues so that they can be compared. For alanine and glycine, the energy differences were −129 kJ mol^{-1} and −46 kJ mol^{-1}, respectively (see Table 1). Thus, the energy difference for helix formation is significantly larger for valine than for alanine. The multicanonical Monte Carlo studies of Okamoto and Hansmann[30] (see Table 7) indicated that the $T\Delta S$ term for helix formation is less unfavorable for valine polypeptides than for alanine, and this may also contribute to the difference in the helix-forming properties of the alanine and valine peptides. Note, however, that Okamoto and Hansmann found the ΔH of helix formation to be smaller for valine than for alanine. This difference presumably resulted from the different force fields employed. Okamoto and Hansmann used the ECEPP/2 force field.[74,75]

In previous work, we have argued that the energy difference between the helix and random globule is larger in the alanine-based peptides than in their glycine analogues because glycine makes better random globules.[27] The network of hydrogen bonds that establishes the helical conformation should be very similar in glycine and alanine. However, glycine, with no side chain and more conformational freedom, is able to make more-compact random globules with a lower strain energy. A similar argument can be used to rationalize why the energy difference for helix formation in valine-based peptides is larger than in the alanine analogues. With its bulky side chain, valine makes worse (less compact and higher energy) random globules than alanine. The energy difference between the valine and the alanine globules can explain why the weak helix formers are helical for valine and are not for alanine.

As noted in the Introduction, valine's low helix propensity in aqueous solution has been rationalized in terms of side chain entropy (or crowding in the helical conformation).[31] The observation that valine apparently has a high helix propensity in vacuo suggests that side-chain entropy is probably not the cause of the low propensity in aqueous solution. The low propensity in aqueous solution is presumably due to interactions with the solvent. A valine helix has large hydrophobic side

(74) Nemethy, G.; Pottle, M. S.; Scheraga, H. A. *J. Phys. Chem.* **1983**, *87*, 1883−1887.
(75) Sippl, M. J.; Nemethy, G.; Scheraga, H. A. *J. Phys. Chem.* **1984**, *88*, 6231−6233.

chains pointing to the outside. In aqueous solution, this will destabilize the helix relative to the random coil, in which some of the side chains can be buried.

An issue we have not considered thus far is whether the peptides retain a memory of their solution phase conformations after being introduced into the gas phase. Although valine has a low helix propensity in aqueous solution, recent measurements show that valine can have a much higher helix propensity in a nonpolar solvent (*n*-butanol).[76,77] How the helix propensities are affected by the solvent, primarily trifluroacetic acid, employed in this work is not known or easily determined. The highly acidic environment used here might be expected to disrupt helix formation. Furthermore, in trifluoroethanol, which promotes helix formation, the helix propensity of valine still remains significantly below that of alanine.[78] The hydrophobic peptides examined here are difficult to dissolve in other solvents, so we are currently examining the question of solvent-memory effects with water-soluble peptides.

As noted above, recent measurements of the helix propensities of the commonly occurring amino acids in a nonpolar solvent, *n*-butanol, show that valine has a much higher helix propensity than in aqueous solution.[76,77] The rank ordering of helix stabilities deduced from our work, valine > alanine > glycine, tracks the helix propensities found in *n*-butanol. Cell membranes are an important nonpolar environment in real biological systems. The transmembrane segments of proteins are usually helical, even though they contain a large proportion of residues normally considered to be helix breakers, such as valine. This illustrates the importance of understanding helix formation in different environments, and the logical starting point for these efforts is to comprehend helix formation in vacuo.

Conclusions

We have examined the conformations of a variety of valine-based peptides in vacuo using high-resolution ion mobility measurements and molecular dynamics simulations. Ac-Val_n-Lys$+H^+$ and Ac-Val_n+H^+ peptides with more than seven residues are helical. Val_n-Gly-Gly-Val_m+H^+, Val_n-^{L}Pro-Gly-Val_m+H^+, Val_n-^{D}Pro-Gly-Val_m+H^+, and Arg-Val_n+H^+ are random globules. For Val_n+H^+ and Ac-Lys-Val_n+H^+ (and probably Ac-Val_n-Gly-Lys-Val_m+H^+), the smaller peptides are random globules and the larger ones are helical. Although valine has a high propensity to form β-sheets in aqueous solution, the β-hairpin does not appear to be a stable conformation for valine-based peptides in vacuo.

Valine has a low helix propensity in aqueous solution, and several peptides that were not expected to be helical were found to be helical in vacuo. In these peptides, we believe that the C-terminus is protonated, which stabilizes the helical state. Although the C-terminus is less basic than the N-terminus and the lysine side chain, the energy penalty of protonating the C-terminus is recovered by the energy gained from helix formation. The alanine analogues of these peptides are not helical, which suggests that valine has a higher helix propensity than alanine in vacuo. According to MD simulations, the energy difference between the helix and random globule is larger for valine than for alanine. This could explain why the valine analogues of some peptides are helical, but the alanine analogues are not. The high helix propensity found for valine in vacuo suggests that side-chain entropy is probably not the cause of the low propensity in aqueous solution. In aqueous solution, interactions with the solvent probably destabilize the helical state.

Incorporation of Gly-Gly or Pro-Gly in the middle of a valine peptide destroys the helix, but for Gly-Lys, the helix persists. Pro-Gly disrupts the intra-helical hydrogen bonding framework and significantly reduces the energy difference between the helix and the random globule in MD simulations. Incorporation of Gly-Gly also reduces the energy difference between the helix and the random globule. The decrease is smaller than for Pro-Gly, but it is large enough to explain the absence of the helix for valine-based peptides incorporating Gly-Gly when other factors, such as entropy, are taken into account.

Acknowledgment. We thank Jiri Kolafa for use of his MACSIMUS molecular modeling programs, and for his helpful advice. We gratefully acknowledge the support of the National Institutes of Health.

JA001207V

(76) Liu, L.-P.; Deber, C. M. *J. Biol. Chem.* **1998**, *273*, 23645−23648.
(77) Wang, C.; Liu, L.-P.; Deber, C. M. *Phys. Chem. Chem. Phys.* **1999**, *1*, 1539−1542.
(78) Rohl, C. A.; Chakrabartty, A.; Baldwin, R. L. *Protein Sci.* **1996**, *5*, 2623−2637.